More on the Scattering Function of Helical Wormlike Chains

Kyosuke Nagasaka, Takenao Yoshizaki, Jiro Shimada,† and Hiromi Yamakawa*

Department of Polymer Chemistry, Kyoto University, Kyoto 606, Japan

Received May 9, 1990

ABSTRACT: The scattering function of the helical wormlike (HW) chain, especially in the range of large magnitude k of the scattering vector, is reinvestigated. First, the scattering function for atactic poly(methyl methacrylate) with the fraction of racemic diads $f_r = 0.79$, for which the HW model parameters were already determined, is evaluated for the HW chain having discrete scatterers on its contour, and it is shown that the Kratky plot obtained does not exhibit the second maximum and minimum as observed for the syndiotactic chain (with $f_r = 1.0$). This conclusion is also consistent with Monte Carlo calculations on the basis of the rotational isomeric state model. Then the effect of chain thickness on the scattering function actually observed by small-angle X-ray scattering is evaluated on the basis of the cylinder and touched-spheroid models for electron distribution. The results show that the scattering function depends strongly on the model for the electron distribution in the range of $kd \gtrsim 7$, where d is the diameter of the cylinder. Therefore, it is dangerous to construct the scattering function for the contour from the one actually observed in this range, as has often been done by the use of an approximate formula for the correction of chain thickness.

I. Introduction

On the basis of the helical wormlike (HW) chain,[1,2] we have already made a theoretical study of the scattering function $P(k)$,[3,4] i.e., the form factor as a function of the magnitude of the scattering vector $\mathbf{k}$ for polymer chains without excluded volume in dilute solutions. Although the model itself may rather well mimic the equilibrium conformational behavior of individual real polymer chains on the bond length or somewhat longer scale, the evaluation of $P(k)$ has been carried out in a continuous-point-scatterer approximation. Necessarily, the results cannot be applied to small-angle X-ray scattering (SAXS) or neutron scattering in the range of large k, since $P(k)$ there must depend on the precise spatial distribution of scatterers (electrons or neutrons) through the very local conformation and chemical structure of the chain. Thus the object of the present paper is to reinvestigate $P(k)$ of the HW chain in the large-k region in various respects.

Now our theory[3,4] can predict the first maximum and minimum but not the second ones in the Kratky plot of $P(k)$ as observed by Kirste and Wunderlich[5-7] in the SAXS experiment for syndiotactic poly(methyl methacrylate) (s-PMMA). However, Yoon and Flory[8] carried out Monte Carlo calculations on the basis of the rotational isomeric state (RIS) model[9] and showed the existence of such oscillation for s-PMMA, taking the α-carbon atoms as the scatterers. On the other hand, we have recently determined experimentally the mean-square radius of gyration $\langle S^2 \rangle$ using well-characterized samples of atactic PMMA (a-PMMA), including the oligomers, with the fraction of racemic diads $f_r = 0.79$,[10] and shown that the unusual dependence of $\langle S^2 \rangle$ on the molecular weight M may well be explained by the HW theory. The above disagreement between the HW theory and experiment for $P(k)$ may therefore be regarded as arising from the discrete distribution of the scatterers on the chain contour along with its local conformation characteristic of PMMA. Thus we first examine the effect of such discreteness. We also examine whether the RIS model can give a consistent explanation of the behavior of $P(k)$ and $\langle S^2 \rangle$ for a-PMMA with various values of f_r.

† Present address: NEC Scientific Information System Development, Ltd., Tsukuba, Ibaraki 305, Japan.

In the following paper,[11] we will make an experimental study of $P(k)$ for atactic polystyrene (a-PS) by SAXS measurements to compare the results with the HW theory. Since X-rays are scattered by the atomic electrons in SAXS, their distribution around the chain contour, i.e., the chain thickness, must then be taken into account in the range of large k. Indeed, there have already been proposed several methods for the correction of chain thickness.[7,12,13] However, they do not seem appropriate in the case of flexible polymer chains, considering the approximations made in the theoretical developments. Thus we devise a new method, and its validity will be examined in the following paper by the use of the HW model parameters determined previously for a-PS.[14-16]

The plan of the present paper is as follows. In the next section, the effect of the discrete distribution of scatterers on the HW chain contour is examined. Evaluation is carried out by the use of the weighting function method along with the ϵ method.[17] The validity of these approximation methods is also examined by a comparison of the results with the values obtained for the HW Monte Carlo chains.[10] In section III, $P(k)$ and $\langle S^2 \rangle$ for a-PMMA are evaluated on the basis of the RIS model. In section IV, the scattering function for the HW chain with finite chain thickness is evaluated, and its effect is discussed with some numerical results.

II. Scattering Function for the HW Chain Contour

A. Discrete Scatterers. For convenience, we begin by giving the definition of the four basic HW model parameters. They are the constant curvature κ_0 and torsion τ_0 of the characteristic regular helix taken at the minimum of elastic potential energy, the stiffness parameter λ^{-1} as defined as the bending force constant divided by $k_B T/2$, with k_B the Boltzmann constant and T the absolute temperature, and the shift factor M_L as defined as the molecular weight per unit contour length. (For flexible polymer chains, the torsional force constant may be set equal to the bending force constant; i.e., the Poisson ratio $\sigma = 0$.[1]) In what follows, all lengths are measured as usual in units of λ^{-1} unless specified otherwise.

The scattering function, or form factor, $P(k;L)$ for a general continuous chain (including the HW chain) of total contour length L without excluded volume is given, in the

0024-9297/91/2224-0924$02.50/0

continuous-point-scatterer approximation, by

$$P(k;L) = L^{-2}\langle|\int_0^L e^{i\mathbf{k}\cdot\mathbf{R}(t)}\,dt|^2\rangle = 2L^{-2}\int_0^L (L-t)I(\mathbf{k};t)\,dt \quad (1)$$

where the scatterers are uniformly and continuously distributed on the chain contour, i is the imaginary unit, $\mathbf{R}(t)$ is the end-to-end vector distance for the chain of contour length t ($0 \le t \le L$), $\langle ... \rangle$ denotes an equilibrium configurational average, and $I(\mathbf{k};t)$ is the characteristic function, i.e., the Fourier transform of the distribution function $G(\mathbf{R};t)$ of $\mathbf{R}$

$$I(\mathbf{k};t) = \int G(\mathbf{R};t)e^{i\mathbf{k}\cdot\mathbf{R}}\,d\mathbf{R} \quad (2)$$

The magnitude k of the scattering vector $\mathbf{k}$ is given by

$$k = (4\pi/\lambda_0)\sin(\theta/2) \quad (3)$$

with θ the scattering angle and λ_0 the (reduced) wavelength of the X-rays.

Now, for the present purpose, we consider a continuous chain of contour length L having N identical point scatterers distributed discretely on its contour at intervals of Δt; i.e.

$$L = (N-1)\Delta t \quad (4)$$

For this chain, eq 1 may be replaced by

$$P(k;L) = N^{-2}\langle|\sum_{n=1}^{N}\exp\{i\mathbf{k}\cdot\mathbf{R}[(n-1)\Delta t]\}|^2\rangle = N^{-1} + 2N^{-2}\sum_{n=1}^{N-1}(N-n)I(\mathbf{k};n\Delta t) \quad (5)$$

Thus, as in the case of the continuous-point-scatterer approximation, we must first evaluate $I(\mathbf{k};t)$. This can be done by the use of the weighting function method along with the ϵ method as before.[4]

The weighting function method provides a least-squares approximation to the distribution function $G(\mathbf{R};t)$, as given by eq 4 with eqs 16 and 20 of ref 17; i.e.

$$G(\mathbf{R};t) = \left(\frac{3}{2\langle R^2\rangle}\right)^{3/2} w(\rho)\sum_{m=0}^{s} M_m(t)\rho^{2m} \quad (6)$$

where $w(\rho)$ is a weighting function defined by

$$w(\rho) = \exp[-a_1\rho^2 - a_2\rho - (b\rho^2)^5] \quad (7)$$

with

$$\rho = \left(\frac{3}{2\langle R^2\rangle}\right)^{1/2} R \quad (8)$$

The coefficients a_1, a_2, b, and M_m are functions of the contour length t and the model parameters κ_0 and τ_0. The first three of them are first determined in such a way that the normalized weighting function itself gives the exact moments $\langle R^2\rangle$, $\langle R^4\rangle$, and $\langle R^6\rangle$, and then M_m ($m = 0$–s; $s \ge 3$) are determined in such a way that the $G(\mathbf{R};t)$ given by eq 6 with this w gives the exact moments $\langle R^{2m}\rangle$ ($m = 0$–s). We note that $w(\rho)$ with $a_2 = 0$ is the weighting function of Fixman and Skolnick[18] and that, when $a_2 = b = 0$, eq 6 gives the Hermite polynomial expansion of $G(\mathbf{R};t)$.[9,19,20] From eq 2 with eq 6, we can evaluate $I(\mathbf{k};t)$. The determination of the coefficients above and the integration in eq 2 must be carried out numerically.

For very small t, however, the weighting function method breaks down,[17] and the ϵ method is used. If we define the relative deviation ϵ of R^2 by

$$R^2 = \langle R^2\rangle(1+\epsilon) \quad (9)$$

we have

$$\langle\epsilon^m\rangle = \langle R^{2m}\rangle/\langle R^2\rangle^m - \sum_{r=0}^{m-1}\binom{m}{r}\langle\epsilon^r\rangle \quad (10)$$

so that $\langle\epsilon^m\rangle$ ($m \ge 1$) may be expressed successively in terms of $\langle R^{2r}\rangle$ ($r = 1 - m$). Then we have the sth-order ϵ expansion of I[17,21]

$$I(\mathbf{k};t) = \sum_{m=0}^{s}\frac{(-x)^m}{2^m m!}j_m(x)\langle\epsilon^m\rangle \quad (11)$$

with

$$x = \langle R^2\rangle^{1/2}k \quad (12)$$

where $j_m(x)$ are the spherical Bessel functions of the first kind. We note that $\langle\epsilon\rangle = 0$ and $\langle\epsilon^m\rangle = \mathcal{O}(t^m)$ for $m \ge 2$. The moments $\langle R^{2m}\rangle$ ($m = 1 - s$) required in both methods may be evaluated by an operational method.[22]

The range of t in which the values of I from the two methods converge has already been examined for $s \le 5$ and for various values of κ_0, τ_0, and k.[4,17] It has been found that there exists a common range of t in which the values from the two methods converge together if k is not very large. Thus, for such k, we may obtain accurate values of I over the whole range of t, using the values from the ϵ method for t smaller than some proper small value and from the weighting function method for t larger than that value, both for $s = 5$. With the values of I thus obtained, we calculate $P(k;L)$ from eq 5. The range of k in which I and therefore P can be evaluated depends on the parameters κ_0 and τ_0, and is approximately given by eq 28 of ref 4; i.e., $k \lesssim 10$ for $\kappa_0 = 0$ and $k \lesssim 10 + 2.5(\kappa_0^2 + \tau_0^2)^{1/2}$ for $\kappa_0 \neq 0$. All numerical work has been done by the use of a FACOM M-780 digital computer in this university.

Now we evaluate numerically the scattering function for the HW chain having discrete scatterers on the contour as above. In what follows, we consider the function $F(k;L)$ defined by

$$F(k;L) = Lk^2P(k;L) \quad (13)$$

instead of $P(k;L)$ itself. Note that $F(k;L)$ corresponds to the quantity usually plotted in SAXS and neutron scattering experiments. We have evaluated $F(k;L)$ for the HW chain with the model parameters $\kappa_0 = 4.0$, $\tau_0 = 1.1$, and $\lambda^{-1} = 57.9$ Å, which had been determined from an analysis of experimental data for $\langle S^2\rangle$ for a-PMMA with $f_r = 0.79$.[10] The interval Δt has been chosen to be 0.0476, assuming that the α-carbon atoms are the scattering centers, where we have used the value 36.3 Å^{-1} for M_L. It has been found that the values of F thus evaluated are almost the same as those calculated from eqs 1 and 13 for the HW chain with continuous scatterers down to $L \simeq 1.0$.

B. Monte Carlo Chains. In this subsection, we examine possible errors in $I(\mathbf{k};t)$ calculated in the preceding subsection, comparing the numerical results for $F(k;L)$ above with those evaluated on the basis of the HW Monte Carlo chain[10] with discrete scatterers. We first give a brief description of this chain. It is composed of N_a successive bond vectors $\mathbf{a}_p$ ($p = 1, 2, ..., N_a$) with $|\mathbf{a}_p| = \Delta s$, the pth one being in the direction of the ζ axis of a localized Cartesian coordinate system (ξ,η,ζ) affixed at the contour point $(p-1)\Delta s$, so that $N_a\Delta s = L$. (Note that Δs is not to be confused with Δt.) Let $\Delta\Omega_p$ ($p = 1, 2, ..., N_a - 1$) be the

infinitesimal rotation vector by which the localized coordinate system at the contour point $p\Delta s$ is obtained from the one at the contour point $(p-1)\Delta s$. Then, apart from its entire orientation, the instantaneous configuration of the chain may be specified if a set of vectors $\Delta\Omega_p$ are given. For the generation of $\Delta\Omega_p$, we use the Boltzmann factor e^{-U_p} with U_p the potential energy in units of k_BT associated with the rotation $\Delta\Omega_p$; i.e.

$$U_p = \frac{1}{4\Delta s}[(\Delta\Omega_{p\xi})^2 + (\Delta\Omega_{p\eta} - \kappa_0\Delta s)^2 + (\Delta\Omega_{p\zeta} - \tau_0\Delta s)^2] \tag{14}$$

where $\Delta\Omega_{p\xi}$, $\Delta\Omega_{p\eta}$, and $\Delta\Omega_{p\zeta}$ are the Cartesian components of $\Delta\Omega_p$ expressed in the localized coordinate system at the contour point $(p-1)\Delta s$. Note that U_p given by eq 14 corresponds to the total elastic potential energy of the HW chain of infinitesimally small contour length Δs. The HW Monte Carlo chain thus defined becomes equivalent to the original HW chain in the limit $\Delta s \to 0$, so that Δs must be taken as small as possible. We take $\Delta s = \Delta t/3 = 0.0159$ in the following calculation.

Since the behavior of the scattering function in the range of large k is governed by $I(\mathbf{k};t)$ with small t, we carry out its Monte Carlo evaluation only for small t. In practice, we calculate $P(k;L)$ from the equation

$$P(k;L) = P_1(k;L) + P_2(k;L) \tag{15}$$

with

$$P_1(k;L) = N^{-1} + 2N^{-2}\sum_{n=1}^{n_1}(N-n)\left\langle \frac{\sin[kR(n\Delta t)]}{kR(n\Delta t)} \right\rangle_{MC} \tag{16}$$

$$P_2(k;L) = 2N^{-2}\sum_{n=n_1+1}^{N-1}(N-n)I(\mathbf{k};n\Delta t) \tag{17}$$

where n_1 represents the upper bound on the number of repeat units or scatterers in the chain for which the Monte Carlo calculations are carried out, and $\langle ... \rangle_{MC}$ denotes the Monte Carlo average. Note that $I(\mathbf{k};n\Delta t)$ in eq 17 is evaluated by the weighting function method in the preceding subsection.

We have carried out numerical evaluation for the same a-PMMA chain as in section IIA with $N = 1000$ and $n_1 = 30$, generating 1000 Monte Carlo chains. The results for $F(k;L)$ are shown in Figure 1 along with those for the original HW chain with $L = 999\Delta t$. The solid curve represents the former values and the dashed one the latter. Note that the latter values have been obtained only in the range of k for which the procedure in the preceding subsection is applicable. The methods in the preceding and present subsections are seen to give the values for $F(k;L)$ close to each other in the range of k mentioned above.

It is important to see that for a-PMMA with $f_r = 0.79$, the HW theory does not predict the oscillation of F in the range of large k as observed for s-PMMA, even if the discrete distribution of the scatterers is considered. However, experimental data do not exist for F for the a-PMMA at the present time, and it is not known whether it really exhibits oscillation or not. Thus, in the next section, we examine tentatively the behavior of the scattering function for a-PMMA with various values of f_r on the basis of the RIS model.

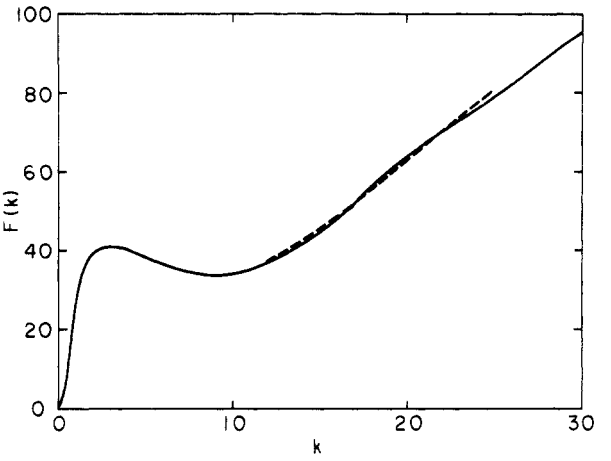

Figure 1. Scattering functions F plotted against the (reduced) magnitude k of the scattering vector for the HW chain with the model parameters $\kappa_0 = 4.0$ and $\tau_0 = 1.1$, which corresponds to a-PMMA with $f_r = 0.79$. The solid curve represents the HW Monte Carlo values with $N = 1000$, $\Delta t = 0.0476$, $n_1 = 30$, and $\Delta s = \Delta t/3$, and the dashed curve the values for the original HW chain with $L = 999\Delta t$.

III. Comparison with the RIS Model

There have been proposed three types of the RIS model for PMMA chains. The two-state model proposed by Sundararajan and Flory[23] is a prototype, and the Monte Carlo calculations carried out by Yoon and Flory[8] are based on it. The three-state model proposed by Sundararajan[24] and the six-state one by Vacatello and Flory[25] are its modifications in which recent data for differences between energies in various rotational states of PMMA chains have been taken into account. We here consider only the two- and three-state models such that both terminal ends are hydrogen atoms. (The six-state model is not considered, for simplicity.) For the RIS chains having such terminal ends, the statistical weight matrices near the ends have already been given in a previous paper.[10] For the matrices for the internal bonds, we use those given in the original papers by the above authors.[23,24]

We first evaluate the scattering function following the procedure of Yoon and Flory.[8] It consists of evaluating the characteristic function for a part of the RIS chain by the Monte Carlo method if the number of repeat units in that part is smaller than or equal to 30, and by the eighth-order Hermite polynomial approximation[9,19,20] otherwise. The scattering function $P(k;x)$, with x the degree of polymerization, is then given by eq 15 with x in place of L and with

$$P_1(k;x) = x^{-1} + 2x^{-2}\sum_{j=1}^{30}(x-j)\left\langle \frac{\sin(kr_j)}{kr_j} \right\rangle_{MC} \tag{18}$$

$$P_2(k;x) = 2x^{-2}\sum_{j=31}^{x-1}(x-j)I(\mathbf{k};j) \tag{19}$$

in place of eqs 16 and 17, respectively, where r_j is the distance between two α-carbon atoms connected by $2j$ successive skeletal bonds, and $I(\mathbf{k};j)$ is given by

$$I(\mathbf{k};j) = \exp\left(-\frac{1}{6}\langle r_j^2\rangle k^2\right)\sum_{m=0}^{4} g_{2m}\left(\frac{1}{3}\langle r_j^2\rangle k^2\right)^m \tag{20}$$

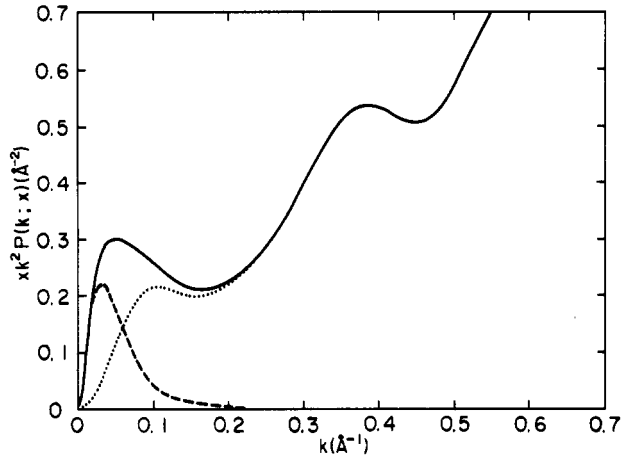

Figure 2. Plots of $xk^2P(k;x)$ (solid curve) against k for the two-state RIS model for s-PMMA at 300 K. The dotted and dashed curves represent the values of xk^2P_1 and xk^2P_2, respectively.

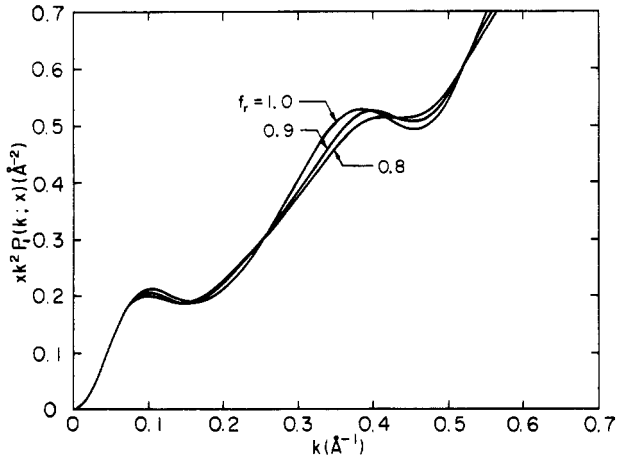

Figure 3. Plots of $xk^2P_1(k;x)$ against k for the two-state RIS model for PMMA with f_r = 1.0, 0.9, and 0.8 at 300 K.

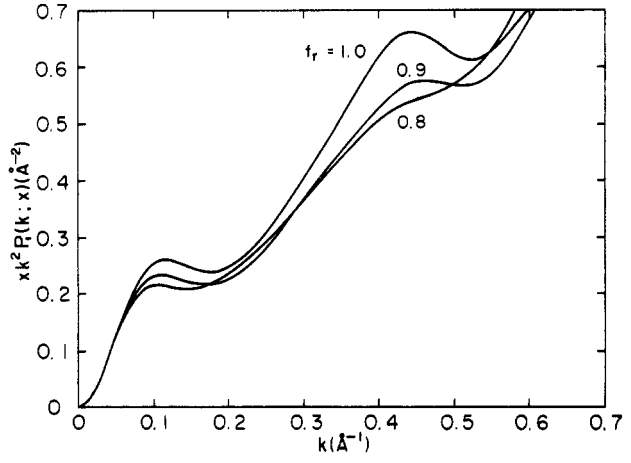

Figure 4. Plots of $xk^2P_1(k;x)$ against k for the three-state RIS model for PMMA with f_r = 1.0, 0.9, and 0.8 at 300 K.

with

$$g_{2m} = 1 \quad \text{for } m = 0$$

$$= 2^{-m}\sum_{n=1}^{m}\frac{(-1)^{n-1}}{n!(m-n)!}\left[1 - \frac{3^n\langle r_j^{2n}\rangle}{(2n+1)!!\langle r_j^2\rangle^n}\right] \quad \text{for } m \neq 0 \tag{21}$$

Figure 2 shows plots of $xk^2P(k;x)$ against k along with those of $xk^2P_1(k;x)$ and $xk^2P_2(k;x)$ for the two-state model for s-PMMA (f_r = 1.0). The solid, dotted, and dashed curves represent the values of xk^2P, xk^2P_1, and xk^2P_2, respectively. It is seen that P_2 makes no contribution to P in the range of large k. Thus, for the examination of the behavior of P in such a k region, we only consider P_1, for simplicity.

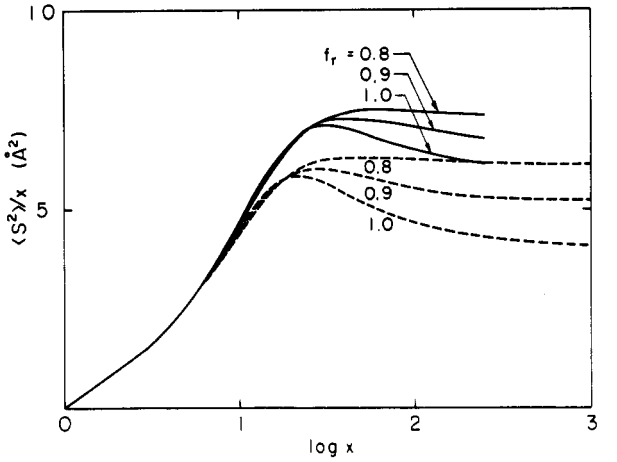

Figure 5. Plots of $\langle S^2\rangle/x$ against log x for the RIS models for PMMA with f_r = 1.0, 0.9, and 0.8 at 300 K. The solid and dashed curves represent the values for the two- and three-state models, respectively.

Figure 3 shows plots of xk^2P_1 against k for the two-state model for s-PMMA (f_r = 1.0) and a-PMMA's with f_r = 0.9 and 0.8. Similar plots are shown in Figure 4 for the three-state model for the corresponding chains. For both models, the amplitude of the oscillation in the range of large k becomes small as f_r is decreased, and the second maximum and minimum almost disappear for f_r = 0.8, although the very weak oscillation is still observed in contrast to the corresponding case of the HW chain.

Now it is instructive to also consider $\langle S^2\rangle$. Figure 5 shows plots of $\langle S^2\rangle/x$ against the logarithm of x for the two models with f_r = 1.0, 0.9, and 0.8. The solid and dashed curves represent the values for the two- and three-state models, respectively. As seen from the figure and as mentioned previously,[10] they fail to predict the remarkable maximum at $x \simeq 50$ observed experimentally for a-PMMA with f_r = 0.79, whereas the HW theory succeeds. At least for this case, therefore, the RIS model cannot give a consistent explanation of the behavior of $P(k)$ and $\langle S^2\rangle$. However, it is necessary and interesting to make a precise experimental study of $P(k)$ for the same PMMA samples.

IV. Effects of Chain Thickness

A. Basic Equations. In this section, we take into account the spatial distribution of electrons around the HW chain contour, i.e., the effect of chain thickness. In general, the scattering function for this case, which we designate by $P_s(k;L)$, may be given by

$$P_s(k;L) = \langle|\int \rho(\mathbf{r})e^{i\mathbf{k}\cdot\mathbf{r}}\,d\mathbf{r}|^2\rangle \tag{22}$$

where $\rho(\mathbf{r})$ is the excess electron density of the single polymer chain over that of the solvent at vector position $\mathbf{r}$ normalized as

$$\int \rho(\mathbf{r})\,d\mathbf{r} = 1 \tag{23}$$

Here, we consider two types of electron distribution. One is a uniform electron distribution within a flexible cylinder of contour length L having a uniform circular cross section of diameter d whose center is on the HW contour (cylinder model), and the other is an assembly of identical (touched) oblate spheroids of principal diameters d_b and γd_b ($0 < \gamma \leq 1$) in which the electrons distribute uniformly (touched-

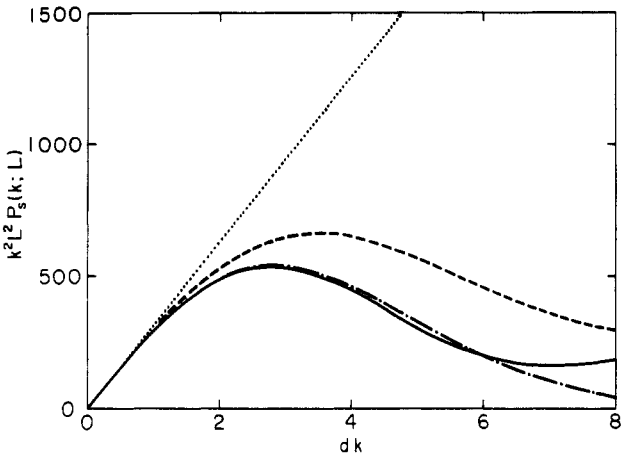

Figure 6. Plots of $k^2L^2P_s(k;L)$ against dk for the rigid rod. The solid curve represents the exact values for the rod of $L/d = 100$ having finite thickness, and the dotted curve for the corresponding rod with vanishing thickness (see text). The dot–dashed and dashed curves represent the approximate values for the same rod with finite thickness calculated by the conventional method for the correction of chain thickness and the method proposed for flexible chains in this work, respectively.

spheroid model).

(i) Cylinder Model. For this model, $\rho(\mathbf{r})$ may be written in the form

$$\rho(\mathbf{r}) = (4/\pi d^2L)\int_0^L dt \int_{C_t} d\mathbf{r}_t\, \delta(\mathbf{r}-\mathbf{R}_t-\mathbf{r}_t) \qquad (24)$$

where $\mathbf{R}_t$ is the vector position of the contour point t, $\mathbf{r}_t$ is the vector distance from this point to an arbitrary point in the normal cross section at the contour point t, $\delta(\mathbf{r})$ is the three-dimensional Dirac δ function, and $\int_{Ct}d\mathbf{r}_t$ indicates the integration over the cross section. Substitution of eq 24 into eq 22 leads to

$$P_s(k;L) = 2L^{-2}\int_0^L (L-t)I_s(\mathbf{k};t)\, dt \qquad (25)$$

where $I_s(\mathbf{k};t)$ is given by

$$I_s(\mathbf{k};t) = (4/\pi d^2)^2\langle \int_{C_0} d\mathbf{r}_0 \int_{C_t} d\mathbf{r}_t \exp\{i\mathbf{k}\cdot[\mathbf{R}(t)+\mathbf{r}_t-\mathbf{r}_0]\}\rangle \qquad (26)$$

with $\mathbf{R}(t)$ being the end-to-end vector distance of the chain of contour length t, as before. The equilibrium average $\langle ... \rangle$ in eq 26 is explicitly given by

$$\langle ... \rangle = (8\pi^2)^{-1}\int d\mathbf{R}\, d\Omega_t\, d\Omega_0\, G(\mathbf{R},\Omega_t|\Omega_0;t)... \qquad (27)$$

where $G(\mathbf{R},\Omega_t|\Omega_0;t)$ is the Green's function for the HW chain of contour length t, with Ω_t and Ω_0 being the Euler angles defining the orientations of the localized coordinate systems at the contour points t and 0, respectively, with respect to an external coordinate system.[1]

If we first take the average over the orientation of the entire chain, eq 26 may be reduced to

$$I_s(\mathbf{k};t) = 2\pi^{1/2}\sum_{n,n_0,n_t=0}^{\infty}\sum_{m=-2n}^{2n}(-1)^{n+(m+|m|)/2}\times$$
$$[(4n+1)(4n_0+1)(4n_t+1)]^{1/2}\begin{pmatrix}2n & 2n_0 & 2n_t\\ 0 & 0 & 0\end{pmatrix}\begin{pmatrix}2n & 2n_0 & 2n_t\\ m & 0 & -m\end{pmatrix}\times$$
$$F_{n_0}(kd)\, F_{n_t}(kd)\langle j_{2n}(kR)\, Y_{2n}^m(\Theta,\Phi)\bar{\mathcal{D}}_{2n_t}^{(-m)0}(\Omega_t)\rangle' \qquad (28)$$

where $(:::)$ is the Wigner $3-j$ symbol,[26] Y_l^m is the spherical harmonics,[27] $\bar{\mathcal{D}}_l^{mj}$ is the unnormalized Wigner function,[28] and $F_n(kd)$ is a function of kd defined by

$$F_n(kd) = (-1)^n 2\pi^{1/2}(4/\pi d^2)\int_{C_0} j_{2n}(kr_0)\, Y_{2n}^0\left(\frac{\pi}{2},\varphi_0\right) d\mathbf{r}_0 =$$
$$\frac{1}{2}(4n+1)^{1/2}\frac{(2n-1)!!}{(2n)!!}\times$$
$$\sum_{m=0}^{\infty}\frac{(-1)^m\Gamma(^1/_2)}{(m+n+1)m!\Gamma(2n+m+^3/_2)}(kd/4)^{2(m+n)} \qquad (29)$$

with Γ the gamma function. In eqs 28 and 29, (R,Θ,Φ) and $(r_0,\pi/2,\varphi_0)$ are the spherical polar coordinates of the vectors $\mathbf{R}$ and $\mathbf{r}_0$, respectively, expressed in the localized coordinate system at the contour point 0. The prime on $\langle ... \rangle$ in eq 28 indicates the average with the Green's function $G(\mathbf{R},\Omega_t|\Omega_0=0;t)$; i.e.

$$\langle ... \rangle' = \int d\mathbf{R}\, d\Omega_t\, G(\mathbf{R},\Omega_t|\Omega_0=0;t)... \qquad (30)$$

Before we proceed to make further developments, it is convenient to consider the case of rigid rods. For this case, the Green's function $G(\mathbf{R},\Omega_t|\Omega_0=0;t)$ is given by

$$G(\mathbf{R},\Omega_t|\Omega_0=0;t) = (t^2\sin\Theta)^{-1}\delta(R-t)\,\delta(\Theta)\,\delta(\Phi)(\sin\theta_t)^{-1}\times$$
$$\delta(\theta_t)\,\delta(\varphi_t)\,\delta(\psi_t) \quad \text{(rod)} \qquad (31)$$

where $\Omega_t = (\theta_t,\varphi_t,\psi_t)$, and δ is the one-dimensional Dirac δ function. Evaluating the average in eq 28 with eqs 30 and 31, we obtain

$$I_s(\mathbf{k};t) = j_0(kt)\sum_{n_0=0}^{\infty}[F_{n_0}(kd)]^2 + \sum_{n=1}^{\infty}(4n+1)j_{2n}(kt)\times$$
$$\sum_{n_0,n_t=0}^{\infty}(-1)^{n_0+n_t}[(4n_0+1)(4n_t+1)]^{1/2}\times$$
$$\begin{pmatrix}2n & 2n_0 & 2n_t\\ 0 & 0 & 0\end{pmatrix}^2 F_{n_0}(kd)\, F_{n_t}(\mathrm{kd}) \quad \text{(rod)} \qquad (32)$$

Here we note that $j_0(kt)$ is just equal to the characteristic function $I(\mathbf{k};t)$ for the rigid rod of length t and that the sum of $[F_{n_0}(kd)]^2$ over n_0 is equal to the scattering function for the circular disk of diameter d.

The values of $(kL)^2P_s(k;L)$ for the rigid rod calculated from eq 25 with eq 32 as a function of dk for $L/d = 100$ are shown by the solid curve in Figure 6. [Note that the dimensionless quantity $(kL)^2P_s$ is a function of dk and L/d.] For the evaluation of the sums over n, n_0, and n_t in eq 32 and over m in eq 29, we have taken such large upper bounds on these indices that P_s converges in the range of dk displayed in Figure 6. The dotted curve in the figure represents the values of the scattering function $P_s(k;L)$ for the rod with vanishing d, i.e., its contour. Note that $(kL)^2P_s$ for this rod ($d = 0$) is a function of kL but is regarded as a function of $(kd)(L/d) = 100kd$, i.e., kd. It is seen that the scattering function for the rod with finite d becomes much smaller than that for the rod with vanishing d in the range of large dk because of the additional interference due to the spatial distribution of electrons around the contour.

We also examine the behavior of the scattering function P_s obtained by the conventional method for the correction of chain thickness. It is given by[7,12]

$$P_s(k;L) = P(k;L)\exp(-d^2k^2/16) \qquad (33)$$

The factor $\exp(-d^2k^2/16)$ represents approximately the additional interference mentioned above. In Figure 6, the dot–dashed curve represents the values calculated from eq 33 with the use of the contour scattering function $P(k;L)$

for the rod (with $d = 0$). For the rigid rod, eq 33 is seen to give a good approximation to P_s in the range of $dk \lesssim 6$.

For the flexible chain, however, the orientational correlation between the two normal cross sections at two arbitrary contour points diminishes rapidly as the contour distance between them is increased, so that the effect of the additional interference may be considered to become smaller than that for the rigid rod. This decrease in the orientational correlation is represented by the averages $\langle ... \rangle'$ on the right-hand side of eq 28. It can be shown that the averages $\langle j_{2n} ... \rangle$ ($n \geq 1$) diminish much faster than $\langle j_0 ... \rangle$ as t is increased. Thus we neglect the averages with $n \geq 1$, for simplicity. In the case of the rigid rod, this approximation gives the values represented by the dashed curve in Figure 6, which have been calculated from eqs 25 and 32 with neglect of all the terms other than the first (j_0) term on the right-hand side of eq 32. The approximation introduced here is, of course, not a good approximation for the rigid rod, for which the orientational correlation never vanishes even if it is infinitely long.

In order to obtain a tractable formula, we further introduce another approximation, i.e., replace the average $\langle j_0 Y_0^0 \bar{\mathcal{D}}_{2n_t}^{00} \rangle'$ ($= \langle j_0 \bar{\mathcal{D}}_{2n_t}^{00} \rangle'/2\pi^{1/2}$) in eq 28 by $\langle j_0 \rangle' \langle \bar{\mathcal{D}}_{2n_t}^{00} \rangle'/2\pi^{1/2}$. Except for very small contour length t, the end-to-end distance R and the orientation Ω_t may be regarded as independent of each other, and therefore this approximation causes no serious errors for flexible chains. The average $\langle j_0 \rangle'$ is equal to the characteristic function $I(\mathbf{k};t)$

$$\langle j_0(kR) \rangle' = I(\mathbf{k};t) \tag{34}$$

and the average $\langle \bar{\mathcal{D}}_{2n_t}^{00} \rangle'$ is given by

$$\langle \bar{\mathcal{D}}_{2n_t}^{00} \rangle' = g_{2n_t}^{00}(t) \tag{35}$$

with $g_t^{jj'}(t)$ the angular correlation function.[1,29] Then we have for the desired expression for $I_s(\mathbf{k};t)$

$$I_s(\mathbf{k};t) = I(\mathbf{k};t) \sum_{n=0}^{\infty} g_{2n}^{00}(t) [F_n(kd)]^2 \tag{36}$$

where we have used a property of the 3-j symbol.[26] We have examined the convergence of the sum on the right-hand side of eq 36 and found that the summands with $n \geq 2$ may be neglected in the ordinary range of k in which SAXS measurements are carried out.

Finally, we give explicit expressions for g_{2n}^{00} and F_n ($n = 0, 1$), for convenience. They read

$$g_0^{00}(t) = 1 \tag{37}$$

$$g_2^{00}(t) = e^{-6t}[(3\kappa_0^4/4\nu^4) \cos 2\nu t + (3\kappa_0^2\tau_0^2/\nu^4) \cos \nu t + {}^1/_4(3\tau_0^2/\nu^2 - 1)^2] \tag{38}$$

with

$$\nu = (\kappa_0^2 + \tau_0^2)^{1/2} \tag{39}$$

and

$$F_0(x) = 4x^{-2}[1 - \cos (x/2)] \tag{40}$$

$$F_1(x) = 4x^{-3}[x[\cos (x/2) - 1] - 6[\sin (x/2) - 1]] \tag{41}$$

(ii) Touched-Spheroid Model. For this model, $\rho(\mathbf{r})$ may be written in the form

$$\rho(\mathbf{r}) = (6/\pi\gamma d_b^3 N) \sum_{p=1}^{N} \int_{V_p} \delta(\mathbf{r} - \mathbf{R}_p - \mathbf{r}_p)\, d\mathbf{r}_p \tag{42}$$

where $\mathbf{R}_p$ is the vector position of the center of the pth spheroid, $\mathbf{r}_p$ is the vector distance from this point to an arbitrary point within that spheroid, and $\int_{V_p} d\mathbf{r}_p$ indicates the integration within it. We note that the center of the pth spheroid is located at the contour point $t = (p-1)\gamma d_b$ and its axis of revolution coincides with the ζ axis of the localized coordinate system at this contour point. Thus the total number N of spheroids in the HW chain may be related to the total contour length as $(N-1)\gamma d_b = L$. This model corresponds to the HW chain defined in section IIA with the spheroids in place of the point scatterers.

For this electron density, $P_s(k;L)$ may be written in the form

$$P_s(k;L) = N^{-1} I_s(\mathbf{k};0) + 2N^{-2} \sum_{p=1}^{N-1} (N-p) I_s(\mathbf{k};p\gamma d_b) \tag{43}$$

where $I_s(\mathbf{k};p\gamma d_b)$ is given by

$$I_s(\mathbf{k};p\gamma d_b) = (6/\pi\gamma d_b^3)^2 \langle \int_{V_1} d\mathbf{r}_1 \int_{V_{p+1}} d\mathbf{r}_{p+1} \times \exp\{i\mathbf{k}\cdot[\mathbf{R}(p\gamma d_b) + \mathbf{r}_{p+1} - \mathbf{r}_1]\} \rangle \tag{44}$$

As in the case of the cylinder model, if we first take the average over the orientation of the entire chain, eq 44 may be reduced to eq 28 with $p\gamma d_b$ in place of t and with

$$F_n(kd_b) = (-1)^n (2\pi^{1/2})(6/\pi\gamma d_b^3) \int_{V_1} j_{2n}(kr_1)\, Y_{2n}^0(\theta_1,\varphi_1)\, d\mathbf{r}_1 \tag{45}$$

in place of eq 29. In eq 45, (r_1,θ_1,φ_1) are the spherical polar coordinates of the vector $\mathbf{r}_1$ expressed in the localized coordinate system at the contour point 0.

Thus, for the touched-spheroid model, $P_s(k;L)$ is given by eq 43 with eq 36 for I_s with $p\gamma d_b$ in place of t and with eq 45 in place of eq 29, if we make the same approximations as introduced in the previous subsection. As in the case of the cylinder model, the summands with $n \geq 2$ in eq 36 with eq 45 may again be neglected. Explicit expressions for F_0 and F_1 required for numerical calculation are given by

$$F_0(x) = (24/\gamma x^3) \int_0^1 [xf(y)]^2 j_1[xf(y)]\, dy \tag{46}$$

$$F_1(x) = -(12\sqrt{5}/\gamma x^3) \int_0^1 (3y^2 - 1)\{-4 \sin [xf(y)] + xf(y) \cos [xf(y)] + 3 \text{ Si } [xf(y)]\}\, dy \tag{47}$$

where $f(y)$ is given by

$$f(y) = {}^1/_2[1 + (\gamma^{-2} - 1)y^2]^{-1/2} \tag{48}$$

and Si (z) is the sine integral defined by

$$\text{Si } (z) = \int_0^z x^{-1} \sin x\, dx \tag{49}$$

The integrations in eqs 46 and 47 must be carried out numerically.

In the particular case of $\gamma = 1$, F_n ($n \geq 1$) vanish, and F_0 is given by

$$F_0(kd_b) = 24(kd_b)^{-3}[\sin (kd_b/2) - (kd_b/2) \cos (kd_b/2)] \quad (\gamma = 1) \tag{50}$$

Note that the square of this F_0 is just the scattering function for the sphere of diameter d_b. Then eq 43 is the exact expression for the scattering function for the touched-sphere (bead) model, and $P_s(k;L)$ is simply factored into $(F_0)^2$ and the contour scattering function $P(k;L)$ given by

eq 5 with d_b in place of Δt; i.e.

$$P_s(k;L) = P(k;L)[F_0(kd_b)]^2 \quad (\gamma = 1) \qquad (51)$$

This relation has already been derived by Burchard and Kajiwara.[30]

Finally, we consider the relation between the cylinder and touched-spheroid models. If we introduce the requirement that the coefficient of the k^2 term in the expansion of P_s for the former be identical with that for the latter (in the long-chain limit), the squared radius of gyration $(2 + \gamma^2)d_b^2/20$ of the spheroid is identical with the one $d^2/8$ of the circular cross section of the cylinder. Then d_b may be related to d by the equation

$$d_b = \left[\frac{5}{2(2+\gamma^2)}\right]^{1/2} d \qquad (52)$$

In what follows, we use instead of d_b the diameter d from this relation for the touched-spheroid model, for convenience.

B. Numerical Results. Now we examine numerically the behavior of the scattering function $F_s(k;L)$ defined by eq 13 with $P_s(k;L)$ in place of $P(k;L)$ for the two models for the electron distribution, i.e., the cylinder model and the touched-spheroid model defined in section IVA. For the former model, $P_s(k;L)$ is calculated from eq 25 with eqs 36–41, where it must be recalled that the index n in eq 36 does not exceed unity. For the latter, F_s is calculated from eq 43 with eqs 36–38, 46, and 47, where $L = (N - 1)\gamma d_b$ and in eq 36 again $n \leq 1$. As already noted, the difference between the integral in eq 25 and the sum in eq 43 is negligibly small, so that the difference between F_s's for the two models may be regarded as arising from F_n ($n = 0, 1$).

An application of the touched-spheroid model to a real polymer chain requires a remark. We replace a repeat unit of the latter by one spheroid such that its principal diameter γd_b is identical with the contour length per repeat unit, the number of spheroids N being equal to that of repeat units. With the value of γd_b evaluated and that of d properly assigned for a given real polymer, the parameter γ is then calculated from eq 52, and therefore d_b is also determined. For comparison, we also consider the touched-sphere (bead) model of the (approximately) same contour length such that its bead diameter d_b is given by eq 52 with $\gamma = 1$ for a given value of d, although it is too coarse-grained as a discrete model and is not realistic.

Figure 7 shows plots of $F_s(k;L)$ against k for the a-PS chain with $f_r = 0.59$ and $N = 1000$. Its HW model parameters are $\kappa_0 = 3.0$, $\tau_0 = 6.0$, $\lambda^{-1} = 22.5$ Å, and $M_L = 36.7$ Å^{-1}, which have been determined from an analysis of the experimental data for the mean-square optical anisotropy and $\langle S^2 \rangle$.[16] With these values of λ^{-1} and M_L, the value of γd_b is evaluated to be 0.126, and then we have $L = 125.9$. The solid curve represents the values for the cylinder model, and the dashed and dotted curves represent the values for the corresponding touched-spheroid and touched-sphere (bead) models, respectively. Note that the value 0.138 of d is the lowest one for the touched-spheroid model corresponding to $\gamma = 1$. Figure 8 shows similar plots for the cylinder and corresponding touched-spheroid models for the same a-PS chain but with $N = 10$ ($L = 1.134$). We note that if N is not very large, we cannot consider the touched-sphere model of the same contour length, since then the number of spheres is not an integer.

Figures 9 and 10 also show similar plots for the a-PMMA chains with $N = 1000$ and 20, respectively, both with $f_r = 0.79$. The HW model parameters for the a-PMMA have already been given in section IIA, and the value of γd_b is evaluated to be 0.0476. Thus the values of L are 47.55 and 0.9044 for $N = 1000$ and 20, respectively. Recall that there are no appreciable differences between the contour scattering functions for the continuous and discrete scatterers for $L \gtrsim 1.0$. (Figure 10 does not include the case of the

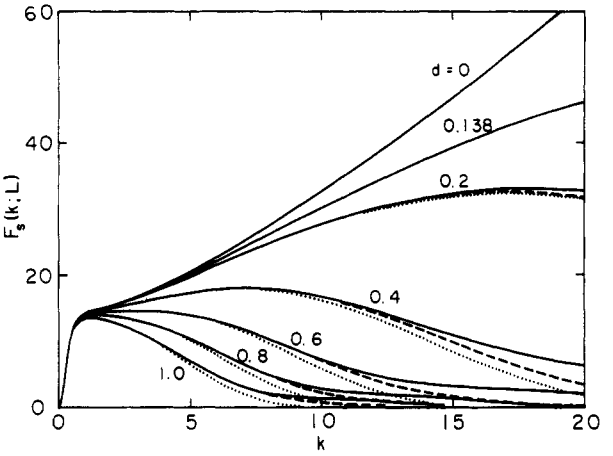

Figure 7. Plots of $F_s(k;L)$ against k for the a-PS chain ($\kappa_0 = 3.0$ and $\tau_0 = 6.0$) with $f_r = 0.59$, $N = 1000$, and $\gamma d_b = 0.126$. The solid curve represents the values for the cylinder model for the indicated values of d, and the dashed and dotted curves the values for the corresponding touched-spheroid and touched-sphere models, respectively (see text).

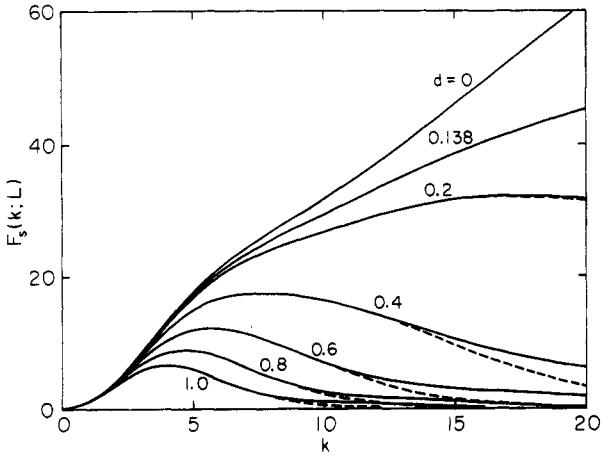

Figure 8. Plots of $F_s(k;L)$ against k for the a-PS chain ($\kappa_0 = 3.0$ and $\tau_0 = 6.0$) with $f_r = 0.59$, $N = 10$, and $\gamma d_b = 0.126$. The solid and dashed curves represent the values for the cylinder model for the indicated values of d and the corresponding touched-spheroid model, respectively (see text).

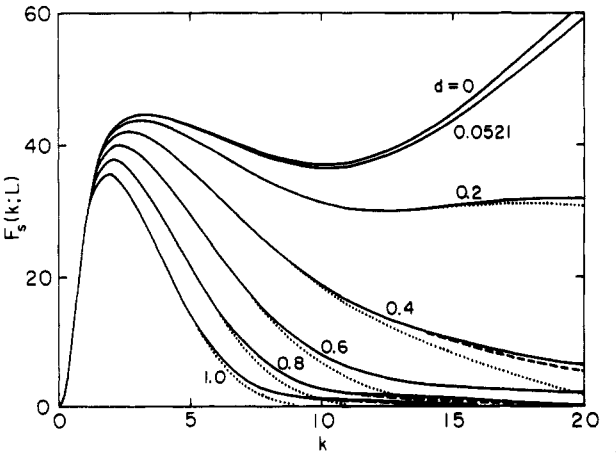

Figure 9. Plots of $F_s(k;L)$ against k for the a-PMMA chain ($\kappa_0 = 4.0$ and $\tau_0 = 1.1$) with $f_r = 0.79$, $N = 1000$, and $\gamma d_b = 0.0476$; see legend for Figure 7.

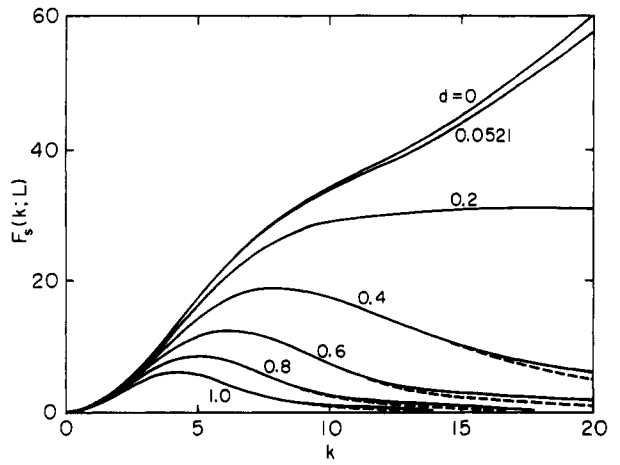

Figure 10. Plots of $F_s(k;L)$ against k for the a-PMMA chain ($\kappa_0 = 4.0$ and $\tau_0 = 1.1$) with $f_r = 0.79$, $N = 20$, and $\gamma d_b = 0.0476$; see legend for Figure 8.

touched-sphere model.)

From the results displayed in Figures 7–10, the following two rather obvious but important facts must be pointed out. First, in the range of small and intermediate k ($kd \lesssim 7$), the actually observed scattering function F_s (with finite chain thickness) is almost independent of the model for the electron distribution but depends on the local configuration of the chain contour, although its initial increase may be described in terms of the Debye function P (for large L). Second, for larger k ($kd \gtrsim 7$), F_s (or its decay) depends strongly on the local electron distribution, so that it is dangerous to construct the scattering function F for the contour from F_s there, as has often been done by the use of an approximate formula for the correction of chain thickness.

V. Concluding Remarks

The behavior of the scattering function for the HW chain has been examined rather in detail, especially in the range of large scattering vector k, giving major attention to two respects. The first is concerned with the contour scattering function F for a-PMMA which may exhibit the second maximum and minimum in this range of k. However, the present analysis shows that both the HW chain and the RIS model fail to predict such behavior of F for a-PMMA with $f_r = 0.79$, for which a maximum has been observed experimentally in $\langle S^2 \rangle / M$ as a function of M.[10] It is therefore premature at the present time to conclude that the oscillation of F is true for this chain before its SAXS experimental study is made to draw the definite conclusion.

The second is the effect of chain thickness, which must be considered in an analysis of experimental data. It has been found that the actually observed scattering function F_s is almost independent of the model for the electron distribution in the range of $kd \leq 7$ but depends strongly on it for larger kd. We note that the above maximum and minimum for a-PMMA, if they occur, will probably do so in the range of $kd \gtrsim 7$, so that the precise electron distribution as well as the configuration of the chain contour must then be considered in order to analyze experimental data for F_s. The validity of the method for the correction of chain thickness proposed here will be examined in the following paper,[11] taking a-PS as an example.

Acknowledgment. This research was supported by a Grant-in-Aid (01430018) from the Ministry of Education, Science, and Culture, Japan.

References and Notes

(1) Yamakawa, H. *Annu. Rev. Phys. Chem.* **1984**, *35*, 23.
(2) Yamakawa, H.; Fujii, M. *J. Chem. Phys.* **1976**, *64*, 5222.
(3) Fujii, M.; Yamakawa, H. *J. Chem. Phys.* **1977**, *66*, 2578.
(4) Yoshizaki, T.; Yamakwawa, H. *Macromolecules* **1980**, *13*, 1518.
(5) Kirste, R. G.; Wunderlich, W. *Makromol. Chem.* **1964**, *73*, 240.
(6) Wunderlich, W.; Kirste, R. G. *Ber. Bunsen-Ges. Phys. Chem.* **1964**, *68*, 646.
(7) Kirste, R. G.; Oberthür, R. C. In *Small Angle X-ray Scattering*; Glatter, O., Kratky, O., Eds.; Academic Press: New York, 1982; p 387.
(8) Yoon, D. Y.; Flory, P. J. *Macromolecules* **1976**, *9*, 299.
(9) Flory, P. J. *Statistical Mechanics of Chain Molecules*; Interscience: New York, 1969.
(10) Tamai, Y.; Konishi, T.; Einaga, Y.; Fujii, M.; Yamakawa, H. *Macromolecules* **1990**, *23*, 4067.
(11) Koyama, H.; Yoshizaki, T.; Einaga, Y.; Hayashi, H.; Yamakawa, H. *Macromolecules*, following paper in this issue.
(12) Porod, G. In *Small Angle X-ray Scattering*; Glatter, O., Kratky, O., Eds.; Academic Press: New York, 1982; p 17.
(13) Koyama, R. *J. Phys. Soc. Jpn.* **1974**, *36*, 1409.
(14) Konishi, T.; Yoshizaki, T.; Shimada, J.; Yamakawa, H. *Macromolecules* **1989**, *22*, 1921.
(15) Einaga, Y.; Koyama, H.; Konishi, T.; Yamakawa, H. *Macromolecules* **1989**, *22*, 3419.
(16) Konishi, T.; Yoshizaki, T.; Saito, T.; Einaga, Y.; Yamakawa, H. *Macromolecules* **1990**, *23*, 290.
(17) Yamakawa, H.; Shimada, J.; Fujii, M. *J. Chem. Phys.* **1978**, *68*, 2140.
(18) Fixman, M.; Skolnick, J. *J. Chem. Phys.* **1976**, *65*, 1700.
(19) Nagai, K. *J. Chem. Phys.* **1963**, *38*, 924.
(20) Jernigan, R. L.; Flory, P. J. *J. Chem. Phys.* **1969**, *50*, 4185.
(21) Fujii, M.; Yamakawa, H. *J. Chem. Phys.* **1980**, *72*, 6005.
(22) Yamakawa, H.; Fujii, M.; Shimada, J. *J. Chem. Phys.* **1976**, *65*, 2371.
(23) Sundararajan, P. R.; Flory, P. J. *J. Am. Chem. Soc.* **1974**, *96*, 5025.
(24) Sundararajan, P. R. *Macromolecules* **1986**, *19*, 415.
(25) Vacatello, M.; Flory, P. J. *Macromolecules* **1986**, *19*, 405.
(26) Edmonds, A. R. *Angular Momentum in Quantum Mechanics*; Princeton University, Princeton, NJ, 1974.
(27) Yamakawa, H. *J. Chem. Phys.* **1973**, *59*, 3811.
(28) Yamakawa, H.; Yoshizaki, T.; Shimada, J. *J. Chem. Phys.* **1983**, *78*, 560.
(29) Yamakawa, H.; Shimada, J. *J. Chem. Phys.* **1979**, *70*, 609.
(30) Burchard, W.; Kajiwara, K. *Proc. Roy. Soc. London* **1970**, *A316*, 185.

Registry No. a-PMMA, 9011-14-7.